Evidence for spin swapping in an antiferromagnet

Lin Weiwei, He Jiaming, Ma Bowen, Matzelle Matthew, Xu Jinsong, Freeland John, Choi Yongseong, Haskel Daniel, Barbiellini Bernardo, Bansil Arun, Fiete Gregory A., Zhou Jianshi, Chien C. L.

DOI: 10.1038/s41567-022-01608-w

Evidence for spin swapping in an antiferromagnet

Weiwei Lin[1†], Jiaming He[2†], Bowen Ma[3], Matthew Matzelle[4], Jinsong Xu[1], John Freeland[5], Yongseong Choi[5], Daniel Haskel[5], Bernardo Barbiellini[6,4], Arun Bansil[4], Gregory A. Fiete[4,7*], Jianshi Zhou[2*], and C. L. Chien[1*]

[1] *Department of Physics and Astronomy, Johns Hopkins University, Baltimore, MD 21218, USA*
[2] *Department of Mechanical Engineering, University of Texas at Austin, Austin, TX 78712, USA*
[3] *Department of Physics, University of Texas at Austin, Austin, TX 78712, USA*
[4] *Department of Physics, Northeastern University, Boston, MA 02115, USA*
[5] *Advanced Photon Source, Argonne National Laboratory, Lemont, IL 60439, USA*
[6] *School of Engineering Science, LUT University, FI-53851 Lappeenranta, Finland*
[7] *Department of Physics, Massachusetts Institute of Technology, Cambridge, MA 02139, USA*

Antiferromagnetic insulators offer strategic advantages in spintronic applications because of their negligible stray fields and ultrafast magnetic dynamics. Here, we report the electrical detection of room temperature magnetization switching in the canted antiferromagnetic insulator $LaFeO_3$, capped with a Pt or W overlayer. The observation of a large magneto-thermovoltage with an in-plane temperature gradient indicates the swapping of spin currents in an antiferromagnet. The magneto-thermovoltage in $LaFeO_3$/(Pt,W) provides a sensitive electrical probe of the tiny net magnetization in the insulator, which can be manipulated by a magnetic field of the order of 10 mT. Our results call attention to a new material class of insulating canted antiferromagnets for spintronics and spin caloritronics and opens the door to the electrical readout of magnetic signals in an antiferromagnetic insulator.

Electrical detection and control of magnetization orientation are central subjects of study in magnetic materials, spin transport, and applications of spintronic devices [1-4]. In ferromagnetic (FM) metals, the magnetization orientation can be electrically switched by using spin transfer torque (STT) and spin-orbit torque (SOT) techniques. The magnetization orientation can be electrically detected via anisotropic magnetoresistance (AMR), the anomalous Hall effect (AHE), and the anomalous Nernst effect (ANE) [5-7]. For ferrimagnetic insulators, such as yttrium iron garnet $Y_3Fe_5O_{12}$ (YIG), the longitudinal spin Seebeck effect (LSSE), and the spin Hall magnetoresistance have been extensively employed to reveal its magnetization orientation [8,9]. It remains far more challenging to switch and detect the vanishingly small net magnetization of antiferromagnetic (AF) materials. The LSSE has been reported in AF insulators, such as Cr_2O_3 and MnF_2, but only in a large applied magnetic field exceeding the spin-flop field—typically several Tesla in magnitude—that induces a canted magnetization in the field direction [10,11]. Subtle quantum effects in some non-collinear AF semimetals, such as the kagome AF Mn_3Sn, allow the AHE and ANE to reveal a small net magnetization [12,13]. However, it is particularly challenging to accomplish electrical detection of sublattice magnetization switching in collinear AF insulators. Evidence of the electrical switching of the Néel vector in AF insulator NiO via an

adjacent heavy metal Pt has been reported [14,15], but the origin of the electrical signals used to detect the switching require care in their interpretations [16,17].

In this work, we combine the electrical detection of magnetization switching with the discovery of a large magneto-thermovoltage resulting from a pure spin current in the canted AF $LaFeO_3$/Pt system with an in-plane temperature gradient. Since the same geometry in our experiment has no out-of-plane signal (*c*-orientated crystal), our work is qualitatively different from earlier studies where thick samples resulted in an out-of-plane temperature gradient when an in-plane gradient was applied [18]. Remarkably, the voltage signal is comparable in magnitude to the celebrated YIG/Pt system, but completely unexpected based on intuition developed for YIG. The crucial difference lies in the nature of the canted magnetism of $LaFeO_3$. In addition, we observe the LSSE in $LaFeO_3$/Pt in the conventional arrangement of a perpendicular temperature gradient for an *ab*-orientated crystal. $LaFeO_3$/W was also studied in the in-plane and perpendicular temperature gradient configurations and produced the expected sign change in the voltage from the opposite sign of its spin Hall angle. Together these results firmly establish a new spin-injection effect, indicating the swapping of spin currents as proposed theoretically [19] in which the spin direction and the direction of magnon/spin current flow are interchanged. The observation of robust signals in an unconventional temperature gradient and magnetic field configuration may open the door to new applications of magneto-thermal/spin caloritronic effects that exploit the feature of lateral spin transport, which may be important for constrained geometries in device miniaturization [20].

In the devices studied, a spin current is detected with the aid of spin-orbit coupling via the inverse spin Hall effect (ISHE), whereby a spin current is injected from a magnetic insulator into a heavy metal. The spin current is converted into an electrical current, which in turn produces charge accumulation on the boundary of the sample and exbibits an associated electrical potential. Prior studies with such a configuration have been made primarily on the combination of Pt and YIG, which has emerged as a standard-bearer in the field [8,9]. However, because of the paltry number of material combinations in which a strong voltage response is observed from an applied temperature gradient driving the spin current, many possible phenomena still remain experimentally unexplored. With our observation of a strong voltage response to an in-plane temperature gradient, our work is an important step in the direction of widening the collection of established phenomena.

The novel magneto-thermoelectric effects we observe in the $LaFeO_3$/Pt system can be attributed to the low-field magnetization switching of the canted antiferromagnetic insulator $LaFeO_3$ in Fig. 1A. $LaFeO_3$ exhibits G-type magnetic ordering below a Néel temperature of 760 K [21-23]. Detailed information about the crystal growth and the characterization is provided in the Supplementary Materials. Figure 1B shows the magnetization in a $LaFeO_3$ crystal with the magnetic field *H* applied along the *a, b,* and *c*-axes. A spontaneous magnetization is observed when the magnetic field is applied along the *a* (the Γ_2 spin structure) and *c*-axes (the Γ_4 spin structure), as illustrated in Fig. S11. The spin canting moment with magnitude of 0.04 μ_B is about 1% of the high-spin Fe^{3+} moment [21,22]; with the expected 5 μ_B on Fe^{3+}, the canting angle is approximately 0.52° [24]. The extremely sharp magnetization switching at the coercive field is

inconsistent with domain wall dynamics [25]; it results from flipping all spins by 180° [26], as illustrated in Fig. 1B. However, when the magnetic field is applied along the *b*-axis, there is no detectable magnetization nor switching, because of the nature of the canting structure. The canted spin structure of $LaFeO_3$ and switching behavior in an external field have consequences for spin injection and underlie our observed unusual magneto-thermovoltage responses. YIG, by contrast, behaves like a normal ferromagnet with a negligible magnetocrystalline anisotropy.

For the electrical detection of magnetization switching in insulating $LaFeO_3$, we deposited a thin metallic film (a few nm in thickness) with weak (Cu) or strong (Pt, W) spin-orbit coupling metals onto polished $LaFeO_3$ by DC magnetron sputtering at room temperature. We first describe the magneto-thermoelectric effect in *a,b*-orientated $LaFeO_3$ single crystals (3 mm × 3 mm and 0.5 mm in thickness) in which the canted moment along the *c*-axis is in the plane parallel to the interface with a 3 nm thick Pt overlayer, as illustrated in Fig. 2A. We measured the transverse magneto-thermovoltage in the *a,b*-oriented $LaFeO_3$/Pt with a vertical temperature gradient T (about 10 K/mm) and an in-plane magnetic field. Figure 2B shows the magnetic loop of the thermovoltage for an in-plane magnetic field applied in various directions within the plane parallel to the Pt layer. The piece-wise constant thermovoltage-magnetic field loops with sharp switching resembles the magnetization loops shown in Fig. 1B. There is no obvious exchange bias effect in these loops. This configuration is a standard LSSE geometry with an out-of-plane temperature gradient and an in-plane magnetic field, as in all previous experiments using magnetic insulators such as YIG/Pt [8,9]. However, as shown in Fig. 2C, the angular dependence of the saturated transverse thermovoltage shows a step-like dependence, rather than the usual sinusoidal behavior observed in YIG/Pt.

The step-like dependence indicates that the thermovoltage in $LaFeO_3$/Pt depends only on the canted magnetization, which is along the *c*-axis in $LaFeO_3$. The magnetization switching field and the angle of applied magnetic field follows a $1/|\cos\alpha|$ dependence as shown in Fig. S5 with a fitting parameter H_c close to the coercive field obtained from the magnetization measurement. Because the magnetization switching field is at its minimum along the *c*-axis, we can easily identify the *c*-axis in the *a,b*-oriented $LaFeO_3$, which is about 30° with respect to the *x*-direction in the plane, as shown by the dotted line in Fig. 2A. Furthermore, we also observed the magneto-thermoelectric effect in $LaFeO_3$/W, which exhibits the opposite sign of the voltage relative to $LaFeO_3$/Pt (Fig. S6A)—consistent with the opposite sign of the spin Hall angle (SHA) in these two heavy metals. In addition, no signal is detected in $LaFeO_3$/Cu. Together, these observations support the conclusion that the signal is an intrinsic LSSE where a vertical (or out-of-plane) temperature gradient drives a spin current $\boldsymbol{J}_S$ with spin polarization $\hat{\boldsymbol{\sigma}}$ across the interface into the Pt (W) layer and the thermal voltage is detected via the inverse spin Hall effect (ISHE) with the *y*-component of a transverse charge current $\boldsymbol{J}_C$ [4,27],

$$\boldsymbol{J}_c = (2e/\hbar)\,\theta_H\,\boldsymbol{J}_S \times \hat{\boldsymbol{\sigma}}, \qquad (1)$$

where e is the electron charge and θ_H is the SHA of Pt (W). The transverse magneto-thermoelectric coefficient is $S = V/(d\,\nabla T)$, where d is the separation of the two voltage probes. The S of the *a,b*-oriented $LaFeO_3$/Pt is about 0.01 μV/K for an out-of-plane temperature gradient in the Fig. 2A configuration. The ratio of the thermovoltage to the canted moment in $LaFeO_3$/Pt is comparable to that of YIG/Pt. When the measurement with the same configuration was applied to a *c*-oriented $LaFeO_3$/Pt, no switching signal was detected (Fig. 2E). This is because the net magnetization remains along the *c*-axis, parallel to $\boldsymbol{J}_S$, giving rise to zero ISHE voltage, and the contribution of Γ_2 magnetization to the LSSE is negligible.

Although the *c*-oriented crystal shows no switching signal in the standard configuration with the vertical temperature gradient, we made remarkable observations on the *c*-oriented crystal with an *in-plane* temperature gradient, as illustrated in Fig. 3. An in-plane temperature gradient would naively only generate a spin current parallel to the interface and not produce a voltage signal, yet we obtain a strong, reproducible (across several devices) response. In the configuration of Fig. 3, a 3 nm Pt (W) layer was deposited on a crystal plate with *a,b*-axes in the plane, a thermal gradient $\boldsymbol{T}$ of 3.3 K/mm was applied along the *x*-direction, and a magnetic field was scanned continuously in the *xy*-plane and along the *z*-axis. Figure 3B shows a large magneto-thermovoltage in the $LaFeO_3$/Pt device. The transverse magneto-thermoelectric coefficient S of the *c*-oriented $LaFeO_3$/Pt is about 0.15 μV/K for the in-plane temperature gradient, which is same order of magnitude of the anomalous Nernst coefficient of Fe. Similar to the configuration with the vertical temperature gradient in Fig. 2, the loop of magneto-thermovoltage versus magnetic field is extremely sensitive to the angle α. A loop with sharp switching is found at α = 0° and 180° and an evolution to asymmetric loops are observed between these two angles. These asymmetric loops are in sharp contrast to symmetric loops centered at zero-field in Fig. 2. It is also important to note that there is no switching taking place at α = 80°, which is consistent with the assignment of the *b*-axis along this direction where no spontaneous magnetization can be obtained in Fig. 1B. Whereas the switching field extracted from Fig. 3B is comparable to the coercive field from the magnetization measurement, the asymmetric loops reflect a strong exchange bias effect at the interface of $LaFeO_3$ and Pt. Again, the thermovoltage magnitude is independent of the component of spontaneous magnetization along the field direction and exhibits a nearly constant value depending on the canted spin direction as in Fig. 3C. These features are rooted in the canting and magnetocrystalline anisotropy of $LaFeO_3$.

The measurement configuration with a magnetic field along the *z*-axis also produces a sharp switching as shown in Fig. 3D, E. The magneto-thermovoltage is reversed with the direction of temperature gradient, as shown in Fig. S8C. When Pt is replaced by W in Fig. 3D the voltage exhibited a loop like Fig. 3E but with opposite polarization (Fig. S6E). As Pt and W has opposite sign of SHA, these results indicate that the ISHE is a key ingredient to convert the thermally injected spin current into an electric potential in the in-plane thermal gradient configuration. Our results in Fig. 3 are different from those in YIG/Pt in which there is no magneto-thermovoltage with the in-plane temperature gradient under either in-plane or perpendicular fields [18,28]. In the configuration of Fig. 3D, the temperature gradient, net

magnetization and voltage are mutually perpendicular, different from the transverse spin Seebeck effect (TSSE) and the nonlocal SSE, where the temperature gradient, net magnetization and voltage are all in-plane [29]. We stress that for $\alpha = 0°$ in Fig. 3A, the magnetic field direction and the thermal gradient are parallel. Thus, if the magnetization is aligned along the magnetic field, this vanishing angle is seemingly against the requirement for the magneto-thermovoltage described by Eq. (1). However, the magnetocrystalline anisotropy of $LaFeO_3$ responsible for the canted moment guarantees the moment does not follow the field as in YIG. One may suspect that the anomalous Hall effect could create a potential in the configuration of Fig. 3D. In order to rule out this possibility, we have replaced the thermal gradient with an electric current; no discernable signal has been found, see Fig. S6I.

We have found a magneto-thermovoltage switching in $LaFeO_3$/Pt(W) with two distinct measurement configurations. With a vertical temperature gradient as in the normal LSSE, the magnitude of the thermovoltage from the *a,b*-oriented $LaFeO_3$/Pt is independent of the field direction, but changes sign once the canting moment switches, in sharp contrast to the sinusoidal behavior observed in YIG/Pt. Since the TSSE reported in prior magnetic insulator/Pt systems has been attributed to the LSSE due to a component of vertical temperature gradient [18], the observation of the thermovoltage switching with the in-plane temperature gradient in the *c*-oriented $LaFeO_3$/Pt(W) is truly remarkable given that no LSSE can be discerned in this device (see Fig. 2E). Evidently, we observe a new intrinsic effect.

To establish the absence of induced magnetic moments due to proximity effects from the $LaFeO_3$ substrate, we have also measured the X-ray magnetic circular dichroism (XMCD) at the Fe $L_{2,3}$ and Pt $L_{2,3}$ edges at room temperature (Fig. S10). No detectable magnetic signal from the interface can be observed in $LaFeO_3$/Pt with an applied field of 0.45 T for Pt and 0.4 T for Fe measurements, indicating both the average magnetization of Fe and the proximity magnetization in Pt are negligibly small (less than 0.03 μ_B per Pt atom and <0.1 μ_B per Fe atom). Together, our XMCD measurements on $LaFeO_3$/Pt as well as the presence of the same unusual magneto-thermoelectric effect in $LaFeO_3$/W and $LaFeO_3$/Cu/Pt (Fig. S6F) indicate that the observed signal is intrinsic to spin injection from the insulating magnetic structure and not due to any known charge current or proximity induced effects.

The well-established LSSE-type measurement and the interpretation are applicable to the *a,b*-oriented $LaFeO_3$/Pt with a vertical temperature gradient. Note that our LSSE results in the intrinsically canted AF $LaFeO_3$ are different from those reported in the high field-induced canting (spin-flop) in AF $Cu_2V_2O_7$ [30] and $DyFeO_3$ [31]. No magneto-thermovoltage for a measurement with an in-plane temperature gradient and any direction of applied magnetic field is expected for the configuration in Fig. 3A,D based on the LSSE mechanism for a magnetic moment that continuously follows the direction of the applied field, such as occurs in YIG [18,28]. Indeed, no pure spin injection thermovoltage has been observed in any FM or AF insulator under an in-plane temperature gradient. Besides the LSSE mechanism, we also considered a situation where a vertical spin current injects from $LaFeO_3$ via the magnon Nernst effect (MNE) as $\boldsymbol{J}_z^x = \alpha_{zx}^x \nabla_x T$, where $\boldsymbol{J}_z^x$ is the *x*-polarized spin current along the *z*-direction, and α_{zx}^x is the magnon Nernst response of the in-plane temperature gradient. However, the *a,b*-plane mirror

symmetry of $LaFeO_3$ imposes $\alpha_{zx}^{x} = 0$ and rules out a possible bulk contribution to the thermal voltage from the MNE (SI). An in-plane temperature gradient creates a magnon current in the *x*-direction with spin polarization along *z*-direction, giving rise to a voltage in the *y*-direction. This might be explained by an interfacial electron-magnon interaction: the thermal magnons scatter with itinerant electrons at the Pt interface during the propagation along the *x*-direction and transfer momenta and spin angular momenta to the electrons inducing a *z*-polarized spin current $\boldsymbol{J}_x^z$. This spin current at the Pt interface then generates a charge current (voltage) along the *y*-direction by ISHE. However, this generic effect has never been reported in other magnetic insulator/heavy metal heterostructures and cannot easily explain the evolution of the signal between 0° and 180° in Fig. 3B.

We propose a spin-torque swapping effect to explain the in-plane temperature gradient results. Because of the mirror symmetry breaking and spin-orbit coupling at the interface, an interfacial Dzyaloshinskii-Moriya interaction (DMI) can arise in the $LaFeO_3$/Pt heterostructure. Similar to the torques arising from the electron flow in a magnetic two-dimensional electron gas with Rashba spin-orbit coupling, when the thermal gradient drives a magnon current $\boldsymbol{j}_m$ near the interface, the DMI produces an effective field-like torque $\boldsymbol{\tau}_{FL} \propto \boldsymbol{m} \times (\hat{\boldsymbol{z}} \times \boldsymbol{j}_m)$ and a damping-like torque $\boldsymbol{\tau}_{DL} \propto \boldsymbol{m} \times \left[(\hat{\boldsymbol{z}} \times \boldsymbol{j}_m) \times \boldsymbol{m}\right]$ [32-34], where $\hat{\boldsymbol{z}}$ is normal to the interface and $\boldsymbol{m}$ is the canted moment (Fig. 4). The interchange of directions of magnon flow and spin index can be due to magnon-magnon or magnon-phonon scattering with spin-orbit interactions.

As $LaFeO_3$ shows a near degeneracy between the Γ_2 and Γ_4 magnetic configurations [35], the damping-like torque $\boldsymbol{\tau}_{DL}$ mediated by the magnon flow can reorient the interfacial spin ordering from Γ_4 to Γ_2 with a canted moment along the *a*-axis, and the changed angular momentum is transferred into Pt/W as an *a*-axis polarized spin current j_z^a by the interfacial electron-magnon interaction. As shown in Fig. S6E, by the ISHE of the heavy metal, this injected spin current is detected as a thermal voltage with opposite signs in Pt and W due to the opposite signs of the SHA in Pt and W. When the out-of-plane magnetic field flips, both the *c*-oriented canted moment $\boldsymbol{m}$ and the magnon current $\boldsymbol{j}_m$ will flip their sign leading to a re-oriented moment along the negative *a*-axis direction and a negative thermal voltage (Fig. 3E and Fig. S6E). When the field is in plane, the canted moment from the original Γ_4 state and $\boldsymbol{j}_m$ as well as the induced torques will not be affected by the field [36], while the Zeeman effect from the magnetic field can flip the re-oriented canted moment in a Γ_2 state (Fig. S11). These two effects will compete with each other when the in-plane field flips. If we attribute the unswitched thermovoltage at an 80° angle in Fig. 4 as arising from the magnetic field lying along *b*-axis, then one cannot flip the Γ_2 or Γ_4 canted moment. Thus, the large exchange bias near 80° (see 45° and 105° of Fig. 3B) can be explained by the exchange coupling at the Γ_4 /Γ_2 domain wall competing against weak Zeeman coupling [37,38]. In addition, the gradually reversed thermal voltage curve around zero

field at 80° reflects a Γ_4 /Γ_2 spin reorientation instead of a magnetic field induced sharp switching. On the other hand, with an out-of-plane thermal gradient, $\hat{z} \times \boldsymbol{j}_m = 0$, thus the thermal voltage will not be affected by the DMI torques and only shows square loops without any notable exchange bias effect in Fig. 2. Such a spin-torque effect provides a consistent interpretation of our experimental results and relies on the specific spin structure and magnetic anisotropy of $LaFeO_3$, which are quite distinct from YIG or any other previously studied material. This explains the absence of a voltage signal from spin injection for an in-plane temperature gradient in prior work. The hallmark of this process, shown in the right side of Fig. 4, is that the spin index rotates 90° when an in-plane magnon current (mediated by interfacial DMI torques) transforms to an out-of-plane spin current. Such a "spin swapping" signal is not expected from the TSSE, nonlocal SSE, nor thermal spin drag [18,39]. The mechanism of a spin structure transition at the interface of $LaFeO_3$/Pt(W) under an in-plane temperature gradient may open a new line of study for spin caloritronic effects.

In summary, for a vertical temperature gradient, we have demonstrated a magneto-thermoelectric detection of magnetization switching in the canted AF insulator $LaFeO_3$ with a Pt or W overlayer at room temperature, with an induced voltage versus canted moment ratio comparable to that in the much-studied YIG/Pt system. The opposite sign of the voltage for W compared to Pt, and the absence of a signal for Cu argues strongly for an intrinsic spin injection effect consistent with a LSSE. We have also observed a strikingly different type of magneto-thermovoltage produced by an in-plane temperature gradient, implying the existence of a swapping of spin current produced by the spin-orbit coupling at the *c*-orientated $LaFeO_3$/Pt(W) interface. Our device provides a sensitive electrical probe of a tiny magnetization in an antiferromagnetic insulator that can be manipulated by a small magnetic field of only 10 mT, uncovering extreme sensitivity for switching-based applications. The observed magneto-thermoelectric effects in such systems will certainly spur further experimental and theoretical investigations, and we hope to widen their scope through the introduction of a new material class for study.

ACKNOWLEDGMENTS

Funding: We gratefully acknowledge support by the US National Science Foundation DMREF Grants No. 1729555 and 1729588, and DMR-1949701. The work of MM, BBA and AB was supported by the US Department of Energy (DOE), Office of Science, Basic Energy Sciences grant number DE-SC0019275 and benefited from Northeastern University's Advanced Scientific Computation Center (ASCC) and the NERSC supercomputing center through DOE grant number DE-AC02-05CH11231. This research used resources of the Advanced Photon Source, a DOE Office of Science User Facility operated by the Argonne National Laboratory under Contract No. DE-AC02-06CH11357.

Author contributions: JSZ, WWL, GAF, and CLC conceived the research plan; JMH and JSZ grown the $LaFeO_3$ crystals, performed crystal characterizations, oriented and polished the crystal pellets; WWL and JSX fabricated the devices and performed the magneto-thermovoltage measurements; BM and GAF carried out the modelling and theoretical work; MM, BB, and AB performed the DFT calculations; JF, YC, and DH performed the XMCD measurements. All coauthors contributed to the data analysis and writing of the manuscript.

† These authors contributed equally to this work.

Communication authors: g.fiete@northeastern.edu or jszhou@mail.utexas.edu or clchien@jhu.edu

Data Availability Statement:

Raw data were generated at Johns Hopkins University, University of Texas at Austin, Argonne National Laboratory and Northeastern University. Derived data supporting the findings of this study are available from the corresponding author upon request.

Methods:

Crystal growth and initial characterizations:

Single crystals of $LaFeO_3$ were grown by the travelling solvent floating zone (TFSZ) technique with an image furnace (NEC SC-M35HD). A starting ceramic rod of $LaFeO_3$ was prepared by a solid-state reaction of La_2O_3 (Alfa Aesar, 99.99%) and Fe_2O_3 (Alfa Aesar, 99.99%) in a molar ratio of 1:1, the oxides are thoroughly mixed and calcined at 1250 °C. The crystal growth was carried out with continuous air flow as gas environment, and the growth speed was around 8 mm/h. The obtained single crystal is black in color with a shiny surface. The phase purity of the obtained $LaFeO_3$ is confirmed by powder X-ray diffraction. $LaFeO_3$ has a *Pbnm* (No. 62) space group with lattice parameters of a = 5.566 (2) Å, b = 5.554 (3) Å, c = 7.861 (2) Å. The crystal orientation as well as crystal quality was determined by Laue back reflection. The oriented crystals were polished with lapping films with the grade 30 μm to 0.1 μm to obtain a flat and shiny surface. After polishing, Raman spectra were taken with a confocal Renishaw inVia Raman microscope with a 532 nm wavelength and 10 mW power laser. X-Ray

Photoelectron Spectroscopy (XPS) spectra of polished surface was taken in the vacuum chamber of Kratos XPS system, XPS spectra of in-situ cleaved crystal was also taken for comparison. Magnetization measurements were carried out in a Vibrating Sample Magnetometer (VSM) with Physical Property Measurement System (PPMS) from Quantum Design.

Device fabrication and measurements:

A heavy metal layer of Pt or W was deposited on the polished crystal pellets by DC magneton sputtering at room temperature. The deposition rate of the metal layer was calibrated by the film thickness measured by X-ray reflectivity. The magneto-thermovoltage measurements were performed using a nanovoltmeter and a rotatable electromagnet. The $LaFeO_3$/Pt(W) devices were attached to a resistive heater as the hot side and a Cu plate as the cold side. The temperatures of the sample were checked by the resistance of the Pt stripes deposited on the $LaFeO_3$ crystal. In a typical measurement with a vertical temperature gradient, the temperature difference on the direction of the sample's thickness is about 5 K (the temperature gradient is about 10 K/mm), whereas it is about 10 K (the temperature gradient is about 3.3 K/mm) crossing the crystal plate in the configuration of in-plane temperature gradient.

First-principles calculations:

First-principles calculations within density functional theory (DFT) were carried out on $LaFeO_3$ using the pseudopotential projector-augmented wave method [40] implemented in the Vienna ab initio simulation package (VASP) [41,42]. The implementation of the exchange correlation functional used was that of Perdew-Burke-Ernzerhof (PBE) [43]. A plane wave basis set cutoff of 600eV was chosen and atomic positions and lattice parameters of the $LaFeO_3$ unit cell were relaxed from experimental values until the forces on each atom were below 0.008 eV/ Angstrom. Self-consistency was concluded when the energy difference between subsequent electronic calculations was less than 0.1 μeV. Calculations were done on a Γ-centered grid of 12×12×8 reciprocal space points. Typically, these calculations include a Hubbard U term to better model the effects of electronic correlation. We find that calculations without the term correctly lead to an AFM insulator ground state.

The initial relaxation assumes collinear magnetism and is performed with the conjugate-gradient algorithm implemented in VASP. However, after optimizing the atomic positions and lattice parameters, we allow a non-collinear magnetic structure and include spin-orbit coupling self-consistently [44]. Previous non-collinear DFT calculations have been performed for $LaFeO_3$ [45]. However, unlike previous works, the present calculations have been performed fully self-consistently. To find the correct ground state, we performed calculations with different initial conditions. We initialized the Fe magnetic moments along a different lattice parameter in each of the calculations. The calculated non-collinear magnetic orders are consistent with other theoretical studies and agree with experimental findings [46].

REFERENCES AND NOTES

1 Hirohata, A. *et al.* Review on spintronics: Principles and device applications. *Journal of Magnetism and Magnetic Materials* **509**, 166711, (2020).

2 Manchon, A. *et al.* Current-induced spin-orbit torques in ferromagnetic and antiferromagnetic systems. *Reviews of Modern Physics* **91**, 035004, (2019).

3 Baltz, V. *et al.* Antiferromagnetic spintronics. *Reviews of Modern Physics* **90**, 015005, (2018).

4 Sinova, J., Valenzuela, S. O., Wunderlich, J., Back, C. H. & Jungwirth, T. Spin Hall effects. *Reviews of Modern Physics* **87**, 1213-1260, (2015).

5 McGuire, T. & Potter, R. Anisotropic magnetoresistance in ferromagnetic 3d alloys. *IEEE Transactions on Magnetics* **11**, 1018-1038, (1975).

6 Pugh, E. M. & Rostoker, N. Hall Effect in Ferromagnetic Materials. *Reviews of Modern Physics* **25**, 151-157, (1953).

7 Smith, A. W. The Hall Effect and the Nernst Effect in Magnetic Alloys. *Physical Review* **17**, 23-37, (1921).

8 Uchida, K.-i. *et al.* Observation of longitudinal spin-Seebeck effect in magnetic insulators. *Applied Physics Letters* **97**, 172505, (2010).

9 Uchida, K. *et al.* Thermoelectric Generation Based on Spin Seebeck Effects. *Proceedings of the IEEE* **104**, 1946-1973, (2016).

10 Seki, S. *et al.* Thermal Generation of Spin Current in an Antiferromagnet. *Physical Review Letters* **115**, 266601, (2015).

11 Wu, S. M. *et al.* Antiferromagnetic Spin Seebeck Effect. *Physical Review Letters* **116**, 097204, (2016).

12 Nakatsuji, S., Kiyohara, N. & Higo, T. Large anomalous Hall effect in a non-collinear antiferromagnet at room temperature. *Nature* **527**, 212-215, (2015).

13 Ikhlas, M. *et al.* Large anomalous Nernst effect at room temperature in a chiral antiferromagnet. *Nature Physics* **13**, 1085-1090, (2017).

14 Chen, X. Z. *et al.* Antidamping-Torque-Induced Switching in Biaxial Antiferromagnetic Insulators. *Physical Review Letters* **120**, 207204, (2018).

15 Moriyama, T., Oda, K., Ohkochi, T., Kimata, M. & Ono, T. Spin torque control of antiferromagnetic moments in NiO. *Scientific Reports* **8**, 14167, (2018).

16 Chiang, C. C., Huang, S. Y., Qu, D., Wu, P. H. & Chien, C. L. Absence of Evidence of Electrical Switching of the Antiferromagnetic Nèel Vector. *Physical Review Letters* **123**, 227203, (2019).

17 Churikova, A. *et al.* Non-magnetic origin of spin Hall magnetoresistance-like signals in Pt films and epitaxial NiO/Pt bilayers. *Applied Physics Letters* **116**, 022410, (2020).

18 Meier, D. *et al.* Longitudinal spin Seebeck effect contribution in transverse spin Seebeck effect experiments in Pt/YIG and Pt/NFO. *Nature Communications* **6**, 8211, (2015).

19 Lifshits, M. B. & Dyakonov, M. I. Swapping Spin Currents: Interchanging Spin and Flow Directions. *Physical Review Letters* **103**, 186601, (2009).

20 Yu, H., Brechet, S. D. & Ansermet, J.-P. Spin caloritronics, origin and outlook. *Physics Letters A* **381**, 825-837, (2017).

21 Koehler, W. C. & Wollan, E. O. Neutron-diffraction study of the magnetic properties of perovskite-like compounds $LaBO_3$. *Journal of Physics and Chemistry of Solids* **2**, 100-106, (1957).
22 Treves, D. Magnetic Studies of Some Orthoferrites. *Physical Review* **125**, 1843-1853, (1962).
23 White, R. L. Review of Recent Work on the Magnetic and Spectroscopic Properties of the Rare−Earth Orthoferrites. *Journal of Applied Physics* **40**, 1061-1069, (1969).
24 Treves, D. Studies on Orthoferrites at the Weizmann Institute of Science. *Journal of Applied Physics* **36**, 1033-1039, (1965).
25 Reich, S., Shtrikman, S. & Treves, D. Angular Variation of Coercivity in Orthoferrite Single Crystals. *Journal of Applied Physics* **36**, 140-141, (1965).
26 Zhou, J. S., Marshall, L. G., Li, Z. Y., Li, X. & He, J. M. Weak ferromagnetism in perovskite oxides. *Physical Review B* **102**, 104420, (2020).
27 Saitoh, E., Ueda, M., Miyajima, H. & Tatara, G. Conversion of spin current into charge current at room temperature: Inverse spin-Hall effect. *Applied Physics Letters* **88**, 182509, (2006).
28 Kikkawa, T. *et al.* Longitudinal Spin Seebeck Effect Free from the Proximity Nernst Effect. *Physical Review Letters* **110**, 067207, (2013).
29 Tikhonov, K. S., Sinova, J. & Finkel'stein, A. M. Spectral non-uniform temperature and non-local heat transfer in the spin Seebeck effect. *Nature Communications* **4**, 1945, (2013).
30 Shiomi, Y. *et al.* Spin Seebeck effect in the polar antiferromagnet $Cu_2V_2O_7$. *Physical Review B* **96**, 180414, (2017).
31 Hoogeboom, G. R. *et al.* Magnetic order of Dy^{3+} and Fe3+ moments in antiferromagnetic $DyFeO_3$ probed by spin Hall magnetoresistance and spin Seebeck effect. *Physical Review B* **103**, 134406, (2021).
32 Manchon, A., Ndiaye, P. B., Moon, J.-H., Lee, H.-W. & Lee, K.-J. Magnon-mediated Dzyaloshinskii-Moriya torque in homogeneous ferromagnets. *Physical Review B* **90**, 224403, (2014).
33 Pauyac, C. O., Chshiev, M., Manchon, A. & Nikolaev, S. A. Spin Hall and Spin Swapping Torques in Diffusive Ferromagnets. *Physical Review Letters* **120**, 176802, (2018).
34 Saidaoui, H. B. M. & Manchon, A. Spin-Swapping Transport and Torques in Ultrathin Magnetic Bilayers. *Physical Review Letters* **117**, 036601, (2016).
35 Mao, A. J., Tian, H., Kuang, X. Y., Jia, J. W. & Chai, J. S. Structural phase transition and spin reorientation of $LaFeO_3$ films under epitaxial strain. *RSC Advances* **6**, 100526-100531, (2016).
36 Kovalev, A. A. & Zyuzin, V. Spin torque and Nernst effects in Dzyaloshinskii-Moriya ferromagnets. *Physical Review B* **93**, 161106, (2016).
37 Scholl, A. *et al.* Observation of Antiferromagnetic Domains in Epitaxial Thin Films. *Science* **287**, 1014, (2000).
38 Hallsteinsen, I. *et al.* Magnetic domain configuration of (111)-oriented LaFeO3 epitaxial thin films. *APL Materials* **5**, 086107, (2017).

39 Avci, C. O. *et al.* Nonlocal Detection of Out-of-Plane Magnetization in a Magnetic Insulator by Thermal Spin Drag. *Physical Review Letters* **124**, 027701, (2020).
40 Kresse, G. & Joubert, D. From ultrasoft pseudopotentials to the projector augmented-wave method. *Physical Review B* **59**, 1758-1775, (1999).
41 Kresse, G. & Furthmüller, J. Efficient iterative schemes for ab initio total-energy calculations using a plane-wave basis set. *Physical Review B* **54**, 11169-11186, (1996).
42 Kresse, G. & Hafner, J. Ab initio molecular dynamics for open-shell transition metals. *Physical Review B* **48**, 13115-13118, (1993).
43 Perdew, J. P., Burke, K. & Ernzerhof, M. Generalized Gradient Approximation Made Simple. *Physical Review Letters* **77**, 3865-3868, (1996).
44 Steiner, S., Khmelevskyi, S., Marsmann, M. & Kresse, G. Calculation of the magnetic anisotropy with projected-augmented-wave methodology and the case study of disordered $Fe_{1-x}Co_x$ alloys. *Physical Review B* **93**, 224425, (2016).
45 Weingart, C., Spaldin, N. & Bousquet, E. Noncollinear magnetism and single-ion anisotropy in multiferroic perovskites. *Physical Review B* **86**, 094413, (2012).
46 Bousquet, E. & Cano, A. Non-collinear magnetism in multiferroic perovskites. *Journal of Physics: Condensed Matter* **28**, 123001, (2016).
47 Momma, K. & Izumi, F. VESTA 3 for three-dimensional visualization of crystal, volumetric and morphology data. *Journal of Applied Crystallography* **44**, 1272-1276, (2011).

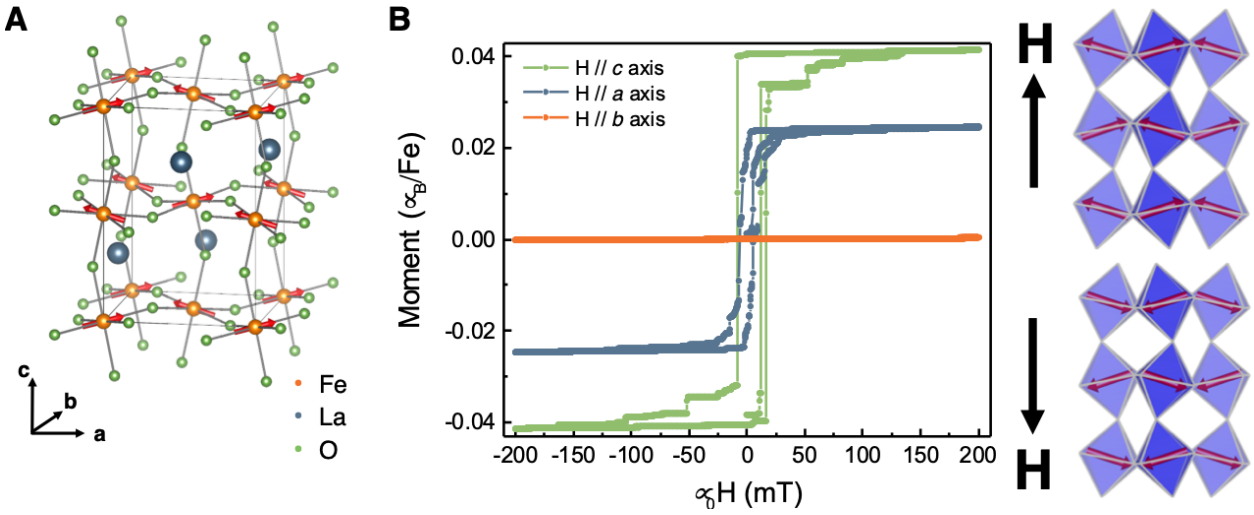

Fig. 1. (A) The crystal and spin structures of perovskite $LaFeO_3$. The red arrows represent the magnetic moments on Fe^{3+}. The easy axis is along the *a* axis of the cell. Spins are slightly canted to the *c*-axis; canting angle in the plot is exaggerated for demonstration. (B) The magnetization loop at room temperature of a $LaFeO_3$ crystal with applied magnetic field along the *a,b,* and *c*-axis. It is difficult to distinguish the *a*-axis and the *b*-axis from a Laue pattern because of $a \approx b$. In this case, we labeled the crystal with *a,b* orientation. However, the sharply different magnetization in (B) helps us assign the crystallographic axes on the crystals we measured. On the right-hand side of (B): a schematic drawing of the spin orientation for the two different magnetization states with respect to different magnetic field direction along the *c* axis. These two states are responsible for the step-like signal in Fig. 2. The structural models were rendered using VESTA [47].

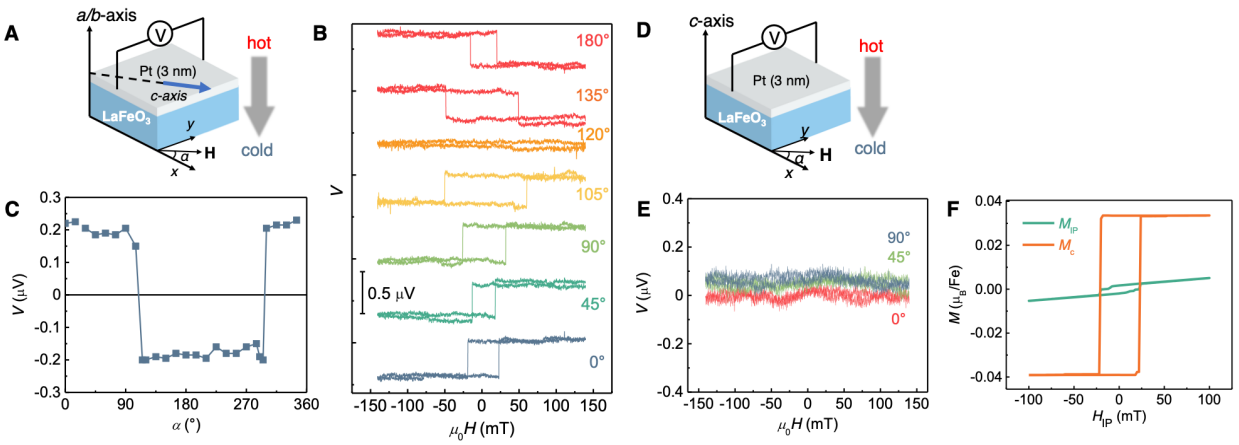

Fig. 2. (A) Schematic of a transverse thermal voltage measurement in the *a,b*-oriented $LaFeO_3$/Pt with an out-of-plane temperature gradient along the *z*-direction and an in-plane applied magnetic field. Blue arrow: direction of spontaneous magnetization in $LaFeO_3$. The angle between the *c*-axis and the *x*-axis is approximately 30°. (B) Magnetic field dependence of the transverse thermovoltage in the *a,b*-oriented $LaFeO_3$/Pt for various in-plane field angles. The voltage for the 120° angle (which is a nearly flat curve) is negative, not zero, and results from the *c*-axis magnetization remaining positive over the magnetic field range shown. (C) Transverse thermovoltage at magnetic saturation as a function of in-plane field angle. The piece-wise constant form is in stark contrast to what is observed in the YIG/Pt system, which shows a continuous dependence on the magnetic field. (D) Schematic of a transverse thermal voltage measurement in the *c*-oriented $LaFeO_3$/Pt with an out-of-plane temperature gradient along the *z*-direction and an in-plane applied magnetic field. (E) Magnetic field dependence of the transverse thermovoltage in the *c*-oriented $LaFeO_3$/Pt in D configuration. (F) Magnetic field dependence of the magnetization of *c*-oriented $LaFeO_3$ with in-plane magnetic field by using vector VSM. The magnetization M_{IP} (green) along in-plane field direction and M_c (orange) along the *c* axis (perpendicular to the field)were measured simultaneously.

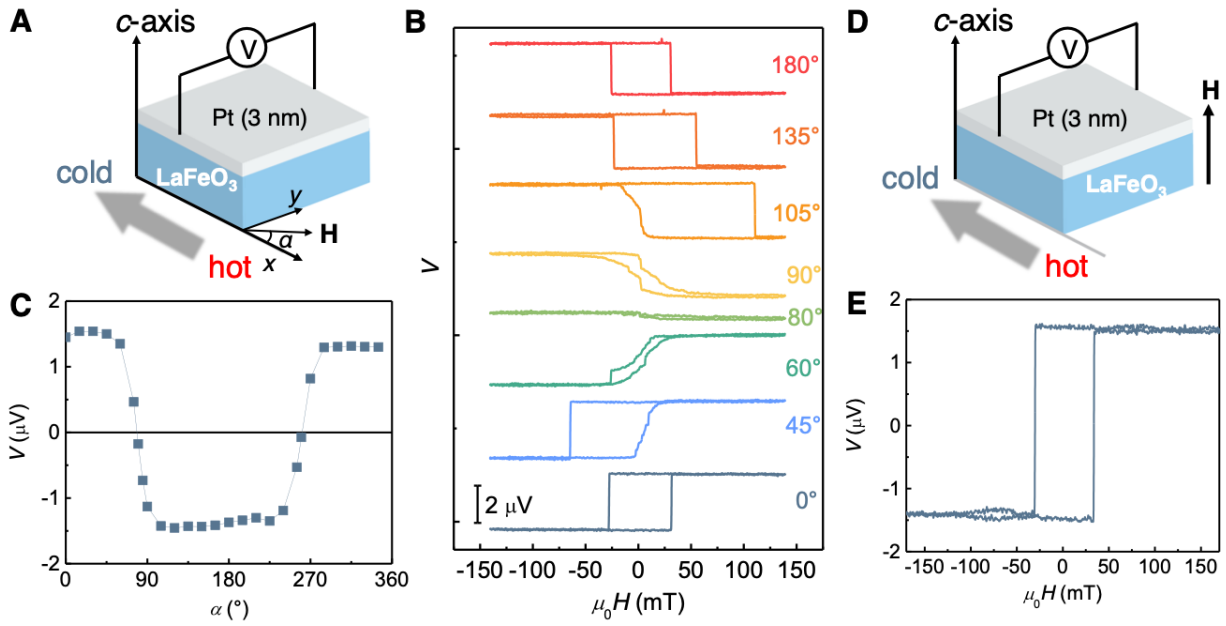

Fig. 3. (A) Schematic of the transverse thermal voltage measurement in *c*-oriented $LaFeO_3$/Pt with an in-plane temperature gradient along the *x*-direction and an in-plane magnetic field. (B) Magnetic field dependence of the transverse thermovoltage in the *c*-oriented $LaFeO_3$/Pt for various in-plane field angles (see Fig. S9 for the results from 180° to 360°) (C) Transverse thermovoltage at magnetic saturation as a function of in-plane field angle. (D) Schematic of transverse thermovoltage measurement in the *c*-oriented $LaFeO_3$/Pt with in-plane temperature gradient and magnetic field along *z* direction. (E) Magnetic field dependence of the transverse thermovoltage from the device in D. Such strong and clear signals have not been previously reported in any system with an in-plane temperature gradient.

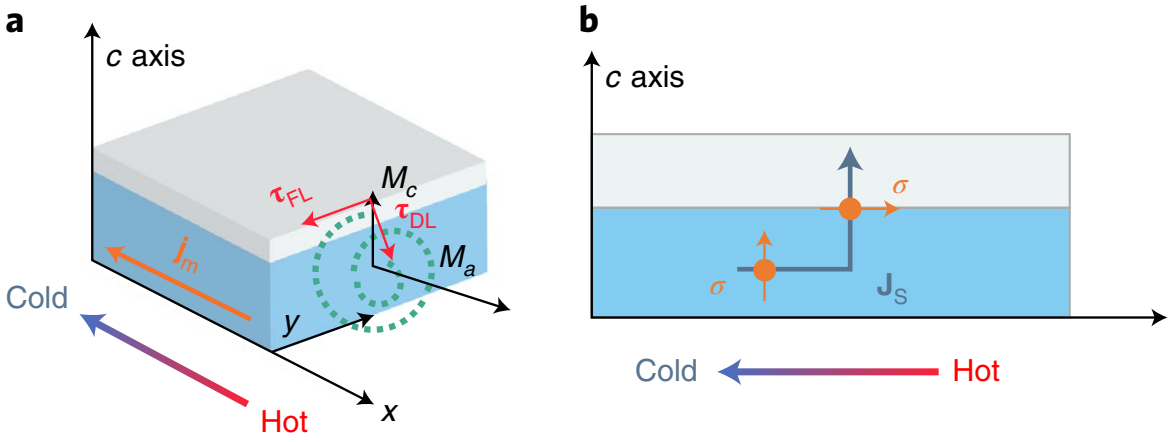

Fig. 4. (Left) Schematic of the spin-torque swapping effect in *c*-oriented $LaFeO_3$/Pt with an in-plane temperature gradient along the *x*-direction. The magnon current $\boldsymbol{j}_m$ is along the temperature gradient (the magnonic spin current is in the opposite direction as the magnon because it carries spin -1). The dotted line shows the trajectory of the magnetic moment. $\boldsymbol{\tau}_{DL}$ ($\boldsymbol{\tau}_{FL}$) is the damping-like (field-like) spin-torque induced by the interfacial Dyzaloshinkii-Moriya interaction swapping the net magnetic moment M_c of Γ_4 to an in-plane moment M_a of Γ_2. The *x*-component of M_a accompanied by a *z*-component of spin-torque induced spin current then contributes to a detectable voltage along *y*-direction by the ISHE. (Right) Schematic of a 90° rotation of spin index and the transformation of an in plane magnon current to an out of plane spin current.